Available online at www.sciencedirect.com
ScienceDirect
Catalysis Today 131 (2008) 76–81
CATALYSIS TODAY
www.elsevier.com/locate/cattod

Synthesis and application of micro-mesoporous SBA-3 with 1,2-bis(triethoxysilyl)ethane as secondary silica source

Fengxi Chen *, He-Kuan Luo, Yi-Fan Han, Cun Wang, Geok Joo Gan

Institute of Chemical and Engineering Sciences, 1 Pesek Road, Singapore 627833, Singapore

Available online 26 November 2007

Abstract

Micro-mesoporous SBA-3 silica (named SBA-3-12) has been successfully synthesized using mixed tetraethyl orthosilicate (TEOS) and 1,2-bis(triethoxysilyl)ethane (BTESE) (12:1 by molar ratio) as silica sources. Its micropore volume and relative ratio of micropore-to-mesopore volume are evidently increased in comparison with SBA-3-∞ synthesized using TEOS as single silica source (0.030 cm^3/g vs. 0.015 cm^3/g and 4.5% vs. 1.9%, respectively). The enhanced microporosity of SBA-3-12 is attributed to the occlusion of some BTESE-derived organic groups into its as-synthesized silica matrix. Upon introducing Ti into SBA-3, Ti-SBA-3-12 shows improved performance in cyclohexene epoxidation with tert-butyl hydroperoxide (TBHP) as compared to Ti-SBA-3-∞ (conversion: 71% vs. 63%; TOF: 33 vs. 27 h^{-1}). This improved performance is attributed to the presence of the micropores inside the mesopore wall that facilitate to expose more Ti sites to substrates.

Keywords: SBA-3; Microporosity; Synthesis; α_s-plot; Epoxidation

1. Introduction

Micro-mesoporous molecular (MMM) sieves possess regular mesopores and amorphous micropore-bearing wall [1,2]. Their applications have been demonstrated in adsorption [3] and catalysis [4,5]. They may be useful for any applications that require (1) high surface area and large pore volume; (2) connected micropores and mesopores; (3) small mass transfer resistance; and (4) enhanced hydroxyl groups for functionalization. One major challenge in Ti-containing mesoporous oxidation catalysts is their low turnover frequency (TOF) because some active Ti centers are buried inside the wall of the mesoporous solid [6]. Ti-containing oxidation catalysts built on the MMM sieves are expected to have improved TOF because the micropores inside the mesopore wall help expose more Ti sites to the reactants [7].

Two methods, i.e., direct synthesis and post-synthesis hydrothermal treatment, have been used to prepare the materials with the above-mentioned unique pore features. Direct synthesis is suitable for SBA-15-based MMM sieves [8–10]. SBA-15 is synthesized with a triblock copolymer $(\text{-PEO-})_{20}(\text{-PPO-})_{70}(\text{-PEO-})_{20}$ as a template. Under low temperatures and acidic conditions, hydrophilic PEO chains of the template penetrate into the silica matrix due to hydration and hydrogen bonding [9,10]. Upon calcination, they form the micropores across the wall of SBA-15, which consists of a micropore-connected hexagonal mesopore system. Similarly, micropore-containing SBA-3 was prepared with the mixture of CTAB and $C_{16}EO_8$ as templates, where the EO groups contribute in part to the formation of the silica pore wall [11]. Post-synthesis hydrothermal treatment [12] comprises two steps: formation of regular mesopore structure and restructuring of the mesoporous surface. Using this method, micropore-containing MCM-41 [13,14], ZSM-5/MCM-41 [5] and ZSM-5/SBA-15 [15,16] have been reported in the literature.

SBA-3-type mesoporous molecular sieves produced from pure TEOS have been demonstrated to possess some micropores inside their mesopore wall [1,2]. In the present work, 1,2-bis(triethoxysilyl)ethane ($(C_2H_5O)_3Si(\text{-}CH_2CH_2\text{-})Si(OC_2H_5)_3$, BTESE) is used to enhance the microporosity of SBA-3. An ethylene group is sandwiched between two terminal triethoxysilyl groups in a BTESE molecule. Therefore, some organic groups (such as $–CH_2CH_2–$ and $–CH_3$) can be occluded into silica network after hydrolysis and co-condensation of silica sources (i.e., TEOS and BTESE), and contribute to the enhanced microporosity upon calcination.

* Corresponding author. Tel.: +65 6796 3825; fax: +65 6316 6182.
E-mail address: Chen_Fengxi@yahoo.com.cn (F. Chen).

0920-5861/$ – see front matter © 2007 Elsevier B.V. All rights reserved.
doi:10.1016/j.cattod.2007.10.035

Upon introducing Ti into SBA-3, the Ti-containing oxidation catalysts based on the MMM sieves show improved performance in cyclohexene epoxidation with tert-butyl hydroperoxide (TBHP) because of the presence of the micropores inside the mesopore wall.

2. Experimental

2.1. Chemicals

Cetyltrimethylammonium bromide (CTAB, Aldrich) and HCl aqueous solution (Baker, 37%) were used as surfactant and pH adjuster, respectively. Tetraethyl orthosilicate (TEOS, Aldrich, 98%) and 1,2-bis(triethoxysilyl)ethane (BTESE, Aldrich, 96%) were used as silica sources. Tetrabutyl titanate (TNBT, 98%) was used as titanium source.

2.2. Preparation of SBA-3-based MMM sieve

A typical procedure is as follows: a clear solution was obtained by dissolving CTAB and HCl in deionized water. TEOS was then added dropwise to this acidic CTAB solution while the mixture was being stirred at 400 rpm and 30 °C. After TEOS hydrolysis for 15 min, an appropriate amount of BTESE was added dropwise. The molar composition of the reaction mixture is CTAB:xTEOS:yBTESE:72.6HCl:1305H_2O, where the silica/CTAB molar ratio is between 8 and 9 and the HCl concentration is 2.7 mM. The molar content of silica in the reaction mixture is calculated to be TEOS + 2 × BTESE. The resulting materials are named SBA-3-n MMM sieves, n indicating the molar ratio of TEOS/BTESE, $R_{t/b}$. After stirring for another 45 min, the resultant white precipitates were filtered without washing and dried at 100 °C overnight. The as-synthesized SBA-3-based MMM sieves were calcined at 550 °C in air for 5 h. The heating rate to 550 °C is 1 °C/min.

2.3. Characterization of SBA-3-based MMM sieves

The mesostructure of the SBA-3-based MMM sieves was checked by powder X-ray diffraction (XRD) patterns, which were recorded on D8 Advance (Bruker AXS GmbH) with Cu Kα radiation at 40 kV and 40 mA. The unit cell, a_o, was calculated from (100) reflection according to the formula $a_o = 2d_{100}/\sqrt{3}$. Wall thickness, t, was calculated by $t = a_o - W_d$, where W_d is geometric mesopore size.

Elemental analysis was carried out on EuroVector Elemental Analyzer (model: EA3011) at furnace temperature of 1030 °C with acetanilide as the standard.

The N_2 adsorption–desorption isotherms were collected on Autosorb-6 at 77 K. For characterization of the microporous features, all isotherms were extended to lower relative pressure (i.e., 1E-05 P/P_0). Prior to the measurements, the samples were degassed at 120 °C until a stable vacuum of 30 mTorr was reached.

The ^{29}Si solid-state magic-angle-spinning (MAS) NMR spectra were collected on Bruker AV400 at room temperature with a resonance frequency of 79.49 MHz. The sample was spun in a 4 mm zirconia rotor at 10 kHz. The relaxation delay was 30 s. Peak position was referenced to tetramethylsilane (TMS). FTIR spectra were measured using KBr pellet on Bio Rad Excalibur 3000 spectrometer with spectrum resolution of 4 cm^{-1}.

The mesopore size distribution (meso-PSD) was calculated using Barrett-Joyner-Halenda (BJH) methods. The specific surface area was assessed using the BET method from adsorption data in a relative pressure range from 0.06 to 0.10. The total pore volume V_t was assessed from the adsorbed amount at a relative pressure of 0.99 by converting it to the corresponding volume of liquid adsorbate with $V_{mi} = v_{mi}c_f$, where c_f is a conversion factor between the volume of gas and liquid adsorbate (when V_{mi} and v_{mi} are expressed in cm^3/g and cm^3 STP/g, respectively, $c_f = 0.0015468$ for N_2 adsorbate at 77 K).

The external surface area S_{ex} (i.e., that of macropores and secondary mesopores), the total surface area S_t (which excludes the surface area of micropores present in the samples), primary mesopore volume V_p and micropore volume V_{mi} were obtained from the high-resolution α_s-plot method [13,14]. LiChrospher Si-1000 (EM Separations, Gibbstown, NJ) served as the macroporous reference adsorbent [17].

The geometric mesopore diameter w_d was calculated from the d_{100} X-ray spacing and the specific primary mesopore volume V_p using the following relation: $w_d = c_d\ (\rho V_p/(1 + \rho V_p))^{1/2}$, where $c = (8/(3^{1/2}\pi))^{1/2} = 1.213$ and $\rho = 2.2$ g/cm^3 is used as the density of pore walls [14].

3. Results and discussion

3.1. Preparation of SBA-3-based MMM sieves

$R_{t/b}$ is critical to form a regular SBA-3 (p6m) mesostructure in its as-synthesized form, i.e., before calcination. Highly ordered SBA-3 (unit cell: 45.5 Å) can be prepared from pure TEOS (Fig. 1a). With the addition of BTESE, the resulting

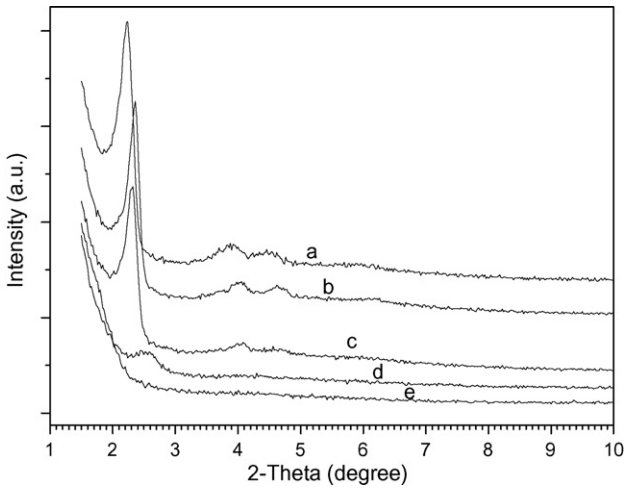

Fig. 1. Powder XRD patterns of as-synthesized samples prepared from CTAB:xTEOS:yBTESE:72.6HCl:1305H_2O. (a) $x = 1$, $y = 0$; (b) $x = 7.2$, $y = 0.6$; (c) $x = 4.6$, $y = 2.2$; (d) $x = 2.8$, $y = 3.3$ and (e) $x = 0$, $y = 8.3$.

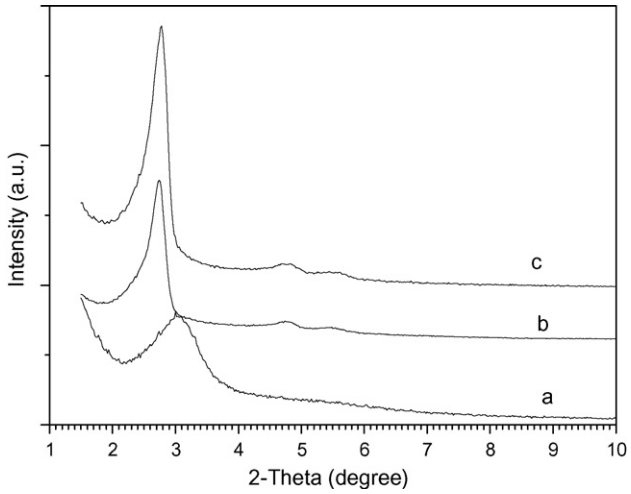

Fig. 2. Powder XRD patterns of calcined samples. (a) SBA-3-6; (b) SBA-3-12 and (c) SBA-3-∞.

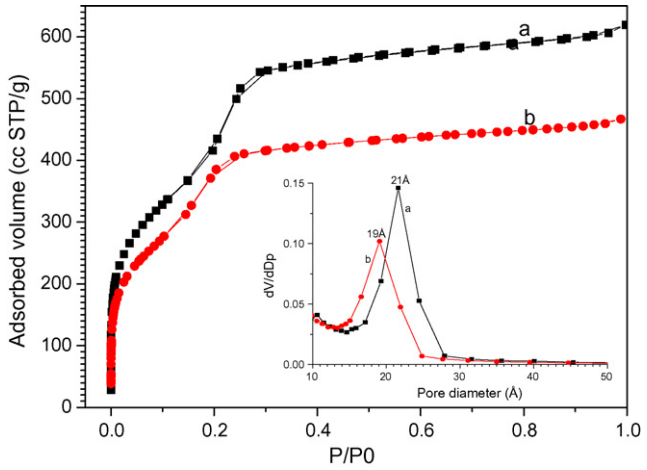

Fig. 3. N_2 adsorption–desorption isotherms of SBA-3-based MMM sieves. (a) SBA-3-∞ and (b) SBA-3-12. Inset is the corresponding PSD curves calculated from BJH model.

samples have smaller unit cell (ca. 43.6 Å), and gradually lose their long-range hexagonal order (Fig. 1c and d). The minimal value of $R_{t/b}$ to form an ordered SBA-3 is 2. Further decrease in $R_{t/b}$ leads to disordered samples (Fig. 1d for $R_{t/b} = 1$ and Fig. 1e for $R_{t/b} = 0$).

After calcination at 550 °C, those samples synthesized with $R_{t/b}$ less than 12 lose their long-range ordered hexagonal mesostructures (see Fig. 2a for SBA-3-6). In Fig. 2b for SBA-3-12, three peaks are observed at $2\theta = 2.78°$, 4.75° and 5.46°, respectively. These are typical (1 0 0), (1 1 0) and (2 0 0) reflections of the 1D hexagonal (p6m) mesostructure with unit cell of 36.7 Å. No distinct XRD peaks are detected at higher angles, suggesting an amorphous silica framework of SBA-3-12. A similar XRD pattern is also observed for SBA-3-∞ except that all three peaks (Fig. 2c) are shifted to lower 2θ angles, indicating a slightly larger unit cell (36.9 Å) of SBA-3-∞ produced from pure TEOS. Elemental analysis results (C: 0.11 wt% for SBA-3-∞ and 0.17 wt% for SBA-3-12, no N detected) show that most of organic components (i.e., CTAB and ethylene groups) have been removed by the current calcination procedure (i.e., 550 °C for 5 h in air). Calcination at higher temperatures causes partial damage or collapse of the ordered SBA-3 mesostructure.

3.2. N_2 adsorption–desorption isotherm

The N_2 adsorption–desorption isotherm of SBA-3-12 is shown in Fig. 3b. It is a reversible type IV isotherm, typical of the mesoporous materials. The step in adsorption between 0.10 and 0.25 P/P_0 is due to capillary condensation in the mesopores. The initial part of the isotherm shows a high "knee" (e.g., the adsorbed volume of liquid N_2 reaches 0.22 cm^3/g at 0.001 P/P_0), followed by a slower growth in adsorbed volume before $P/P_0 = 0.10$. The high "knee" may indicate the presence of the micropore inside SBA-3-12 [3,15]. Its BET surface area and total pore volume are 1192 m^2/g and 0.72 cm^3/g, respectively.

The BJH PSD curve of SBA-3-12 shows an average mesopore size of ca. 19.0 Å (Fig. 3b inset). It is generally agreed that the BJH method underestimates the mesopore size [18]. It is also open to question whether the Kelvin equation is applicable in the current capillary condensation pressure range, i.e., between 0.10 and 0.25 P/P_0. From geometric consideration, the primary mesopore diameter w_d is calculated to be 30.0 Å with the primary mesopore volume $V_p = 0.66$ cm^3/g (estimated from high-resolution α_s-plot shown below).

The N_2 adsorption–desorption isotherm for SBA-3-∞ and its PSD curve (Fig. 3a) have similar features to those for SBA-3-12 except larger values of BET surface area (1435 m^2/g), pore volume (0.96 cm^3/g) and BJH mesopore size (21.0 Å). The geometric mesopore diameter is 31.0 Å with the primary mesopore volume $v_p = 0.80$ cm^3/g. As compared to SBA-3-∞, SBA-3-12 has a slightly larger wall thickness (6.7 vs. 5.9 Å), which may be related to its enhanced microporosity (demonstrated below).

3.3. High-resolution α_s-plot method

The microporous volume of SBA-3 can be assessed from high–resolution α_s-plot (Fig. 4). The initial parts in Fig. 4 bend downwards, indicating the presence of microporosity. The microporous volume, V_{mi}, is estimated by extrapolating the low-pressure linear part (Part I in Fig. 4) before onset of the capillary condensation in primary mesopores (i.e., α_s less than 0.7 in our case) to the "adsorbed volume" axis, and converting the intercept, v_{mi}, to the liquid volume of N_2. Its obvious that SBA-3-12 has a larger amount of micropores than SBA-3-∞ (0.030 vs. 0.015 cm^3/g). The relative content of microporosity to primary mesoporosity in SBA-3-12 is even more than twice higher than that in SBA-3-∞ (4.5% vs. 1.9%). Microporosity of the SBA-3-based MMM sieves is comparable to those of their MCM-41 counterparts (V_{mi}: 0.01–0.041 cm^3/g) prepared via hydrothermal restructuring [13,14].

Additional textual properties (Table 1) can also be obtained from α_s-plot [13,14]. From the slope η_1 of Part I and the BET

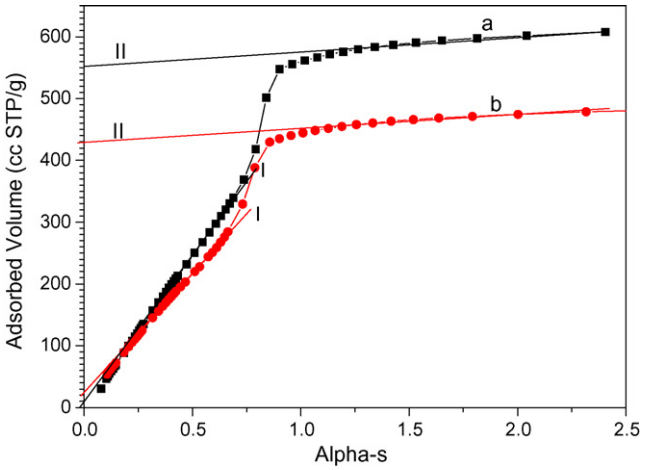

Fig. 4. α_s-plot of SBA-3-based MMM sieves. (a) SBA-3-∞ and (b) SBA-3-12.

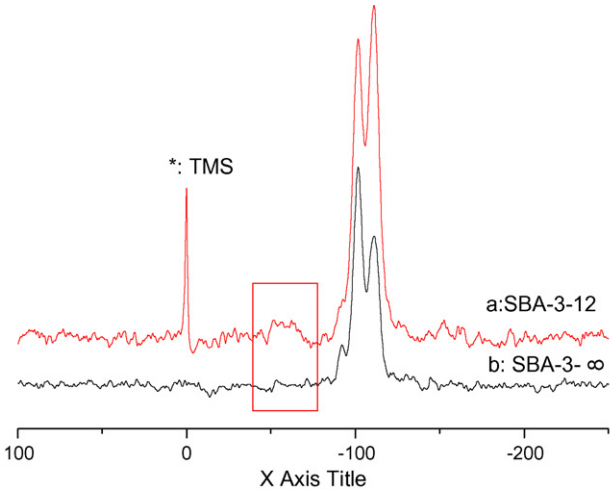

Fig. 5. ^{29}Si solid-state MAS NMR spectra. (a) SBA-3-12 and (b) SBA-3-∞.

surface area of the reference adsorbent LiChrospher Si-1000 silica gel ($S_{BET,ref}$: 25 m^2/g), the total surface area, S_t, is calculated to be 1113 m^2/g for SBA-3-12 and 1300 m^2/g for SBA-3-∞ from $S_t = \eta_1 S_{BET,ref}/v_{0.4,ref}$, where $v_{0.4,ref}$ is the adsorbed volume (9.1248 cm^3/g) at $P/P_0 = 0.4$ for the reference adsorbent. From the intercept, v_p, of the high-pressure linear part (Part II in Fig. 4) after completion of the capillary condensation in primary mesopores (i.e., α_s large than 1.0), the primary mesopore volume, V_p, is calculated to be 0.66 cm^3/g for SBA-3-12 and 0.80 cm^3/g for SBA-3-∞ from $v = v_p + \eta_2\alpha_s$ and $V_p = v_p c_f$, where η_2 is the slope of part II. From the slope η_2 of Part II, the external surface area, S_{ext}, is calculated to be 43 m^2/g for SBA-3-12 and 108 m^2/g for SBA-3-∞ from the formula $S_{ext} = \eta_2 S_{BET,ref}/v_{0.4,ref}$. The primary mesopore surface area, S_p, is estimated from $S_p = S_t - S_{ext}$ to be 1070 m^2/g for SBA-3-12 and 1192 m^2/g for SBA-3-∞.

A fundamental relation exists among the structural parameters for materials with uniform pores of simple circular or hexagonal geometry: $w_d S/V = 4$ or 4.2, respectively, where S and V are defined as the specific surface area and volume of primary mesopores and any other pores of diameters smaller than that of the latter [8]. It is clear that the value of $w_d S/V$ for SBA-3 (i.e., 5.2–5.6) exhibits large deviations from both theoretical values. The observed excess in the specific surface area again indicates the presence of microporosity in SBA-3 [8].

3.4. Origin and location of micropores

As-synthesized SBA-3, i.e., before calcination, is assembled at room temperature (r.t.) under acidic conditions via $S^+X^-I^+$ route, where S^+, X^- and I^+ represent CTA^+, Cl^-/Br^- and silica species, respectively. At r.t. under acidic conditions (pH < 2), silica species consists of positively charged silica oligomers [19]. These oligomers further polymerize upon calcination, and release some small molecules including H_2O and HCl. These molecules may create the micropore in SBA-3 by channeling their way out of silica matrix and/or etching silica wall. The pore roughness and/or corrugation may partly account for the presence of microporosity [8]. In addition, as inferred from the carbon replica technique [11], some micropores may cross-link the primary hexagonal mesopores in SBA-3.

By comparing synthesis procedure of SBA-3-12 and SBA-3-∞, using BTESE as the secondary silica source is the only reason to explain the enhanced microporosity in SBA-3-12. BTESE was previously used to synthesis amorphous [19] and mesostructured [20] porous hybrid materials. Si–C bond has been found in their final products by ^{29}Si CP/MAS NMR spectra. This is also supported in our SBA-3-12 by ^{29}Si MAS NMR spectra (Fig. 5) and FTIR spectra (Fig. 6). A broad peak between −50 and −65 ppm is indicated by a rectangular box in Fig. 5a. It suggests the presence of two types of silicon in silica matrix of as-synthesized SBA-12 via the Si–C bond (i.e., $RSi(OSi)_2OH$ at −55 ppm and $RSi(OSi)_3$ at −65 ppm, R: alkyl groups) [19]. Compared to TEOS-derived silica (Fig. 6a), two additional peaks are observed at 1277 and 1418 cm^{-1} in FTIR spectrum for BTESE-derived silica (Fig. 6b). Both peaks should be due to the presence of some BTESE-derived organic groups since it is the only difference in chemical composition between the TEOS- and BTESE-derived silicas. Two similar peaks are observed in the FTIR spectrum for the as-synthesized

Table 1
Textural properties of SBA-3-based MMM sieves

Sample	S_{BET} (m^2/g)	S_t (m^2/g)	S_{ext} (m^2/g)	S_p (m^2/g)	V_t (cm^3/g)	V_p (cm^3/g)	V_{mi} (cm^3/g)
SBA-3-12	1192	1113	43	1070	0.72	0.66	0.030
SBA-3-∞[a]	1435	1300	108	1192	0.96	0.80	0.015
Ti-SBA-3-12	786	670	12	658	0.47	0.44	0.032
Ti-SBA-3-∞[a]	807	739	13	726	0.52	0.49	0.010

[a] SBA-3-∞ indicates SBA-3 synthesized with pure TEOS.

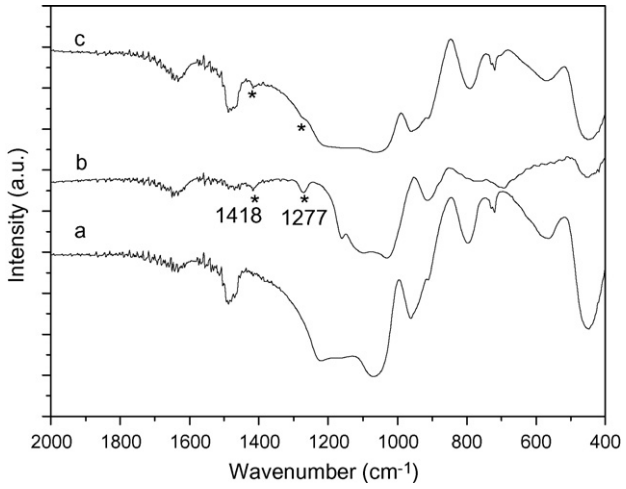

Fig. 6. FTIR spectra of as-synthesized samples prepared from different silica sources. (a) Pure TEOS; (b) pure BTESE and (c) mixed TEOS/BTESE (12:1 by molar ratio).

Table 2
Cyclohexene epoxidation on Ti-SBA-3-n[a]

Sample	Conversion (%)	Ti (wt%)	TOF (h^{-1})
Blank	0	0	N.A.
TS-1	13.6	3.76	1.0
Ti-SBA-3-∞	62.8	0.65	27.1
Ti-SBA-3-12	70.6	0.61	33.0
Ti-SBA-3-0	16.7	0.35	18.0

[a] Reaction conditions: 0.3 g of catalyst, 10 ml of CH_2Cl_2, 1 ml of C_6H_{10} and 1 ml of TBHP (70 wt% in water, dried over anhydrous $MgSO_4$ before use) refluxed in 60 °C oil bath under N_2 for 6 h.

SBA-3-12 (Fig. 6c), indicating that some BTESE-derived organic components are occluded in its silica matrix via the Si–C bond. Upon calcination, these organic components channel their way out of the silicate framework, resulting in the enhanced microporosity in its mesopore wall.

3.5. Epoxidation of cyclohexene over Ti-SBA-3-n

MMM-based Ti-containing oxidation catalysts were made by introducing Ti during hydrolysis and condensation of silica sources into the as-made MMM sieves. These catalysts are tested for cyclohexene epoxidation with tert-butyl hydroperoxide (TBHP) (Table 2). No conversion is observed for blank experiment (i.e., no catalyst) under our reaction conditions. The catalytic performance of different catalysts in terms of C_6H_{10} conversion is in the order of Ti-SBA-3-12 > Ti-SBA-3-∞ > Ti-SBA-3-0 > TS-1 with nearly 100% selectivity to cyclohexene oxide. The sequence in catalytic activity is consistent with the structural and textural features of different catalysts. TS-1 has small micropores (ca. 5.5 Å); its lowest conversion (13.6%) and TOF (1.0 h^{-1}) should be due to diffusion limitation. Ti-SBA-3-0 has a disordered structure with a wide pore size distribution; a small portion of mesopore accounts for its slightly improved performance (conversion: 16.7% and TOF: 18.0 h^{-1}). Conventional Ti-SBA-3-∞ (produced from TEOS only) shows much better activity (conversion: 63% and TOF: 27.1 h^{-1}) because its large mesopore (21.7 Å) overcomes the diffusion limitation. As compared to Ti-SBA-3-∞, Ti-SBA-3-12 with a mesopore size of ca. 19.5 Å shows improved performance (conversion: 71% and TOF: 33.0 h^{-1}). The improved performance of Ti-SBA-3-12 should be due to micropores inside their mesopore wall (Table 1). It should be noted here that it is hard to find a suitable macroporous or non-porous reference adsorbent for comparative studies of Ti-SBA-3 because of the complexity in chemical composition, surface functional groups and pore structure. For simple comparison, the same reference adsorbent as used for SBA-3 silicas (LiChrospher Si-1000) has been chosen to make α_s-plots for different Ti-containing SBA-3 to compare their microporosity. The enhanced microporosity in Ti-SBA-3-12 helps expose more Ti active sites inside the mesopore wall to the reactants in a way somehow like in the case of TS-1. No titanium has been detected by XRF in the filtrate after cyclohexene epoxidation. However, the fact that reaction performance of recycled Ti-SBA-3 gradually deteriorates (cyclohexene conversion reduces to 60.0% and 52.6% for the 1st and 2nd recycled Ti-SBA-3-∞, to 56.5% and 54.5% for the 1st and 2nd recycled Ti-SBA-3-12) suggests that Ti may have leached into the CH_2Cl_2.

4. Conclusions

SBA-3 mesoporous molecular sieve with enhanced microporosity (i.e., microporosity: 0.030 cm^3/g, relative content of microporosity to primary mesoporosity: 4.5%) has been prepared from the initial reaction mixture with a molar composition of CTAB:7.2TEOS:0.6BTESE:72.6HCl:1305H_2O. Using cyclohexene epoxidation with TBHP as a model reaction, Ti-containing oxidation catalysts built on SBA-3 MMM sieves show improved performance as compared to traditional Ti-containing SBA-3 catalysts. The idea used in this work – occlusion of small molecular groups in mesopore framework via chemical interaction (e.g., Si–C bond) – might be extended to be a generic methodology to synthesis a variety of MMM sieves based on different mesoporous structures (e.g., MCM, SBA, HMS, etc.) with new hierarchically structured pore systems and multimodal pore size distributions.

Acknowledgement

F.X. Chen acknowledged the financial support by ICES in-house projects (project codes: ICES/05-112002 and ICES/03-112002).

References

[1] F. Chen, X.J. Xu, S. Shen, S. Kawi, K. Hidajat, Microporous Mesoporous Mater. 75 (2004) 231.
[2] F. Chen, S. Shen, X. Xu, R. Xu, F. Kooli, Microporous Mesoporous Mater. 79 (2005) 85.
[3] C.J. Guo, Stud. Surf. Sci. Catal. 97 (1995) 165.
[4] X. Chen, S. Kawi, Chem. Commun. (2001) 1354.

[5] K.R. Kloetstra, H.V. Bekkum, J.C. Jansen, Chem. Commun. (1997) 2281.
[6] T. Maschmeyer, F. Rey, G. Sankar, J.M. Thomas, Nature 378 (1995) 159.
[7] F. Chen, L. Huang, S. Shen, G.J. Gan, Proceeding in Recent Advances in Catalysis 2005, Rennes, France, (2005), p. 75.
[8] R. Ryoo, C.H. Ko, M. Kruk, V. Antochshuk, M. Jaroniec, J. Phys. Chem. B 104 (2000) 11465.
[9] B.L. Newalkar, S. Komarneni, Chem. Mater. 13 (2001) 4573.
[10] A. Galarneau, H. Cambon, F.D. Renzo, F. Fajula, Langmuir 17 (2001) 8328.
[11] J.-S. Lee, S.H. Joo, R. Ryoo, J. Am. Chem. Soc. 124 (2002) 1156.
[12] D. Khushalani, A. Kuperman, J.J. Olken, N. Coombs, Adv. Mater. 7 (1995) 842.
[13] A. Sayari, M. Kruk, M. Jaroniec, Catal. Lett. 49 (1997) 147.
[14] A. Sayari, P. Liu, M. Kruk, M. Jaroniec, Chem. Mater. 9 (1997) 2499.
[15] D.T. On, S. Kaliaguine, Angew. Chem. Int. Ed. 40 (2001) 3248.
[16] D.T. On, S. Kaliaguine, Angew. Chem. Int. Ed. 41 (2002) 1036.
[17] M. Jaroniec, M. Kruk, J.P. Olivier, Langmuir 15 (1999) 5410.
[18] K. Cassier, P. van Der Voort, E.F. Vansant, Chem. Commun. (2000) 2489.
[19] H.W. Oviatt, K.J. Shea, J.H. Small, Chem. Mater. 5 (1993) 943.
[20] S. Inagaki, S. Guan, Y. Fukushima, T. Shsuna, O. Terasaki, J. Am. Chem. Soc. 121 (1999) 9611.